# Study on Stability and Rotating Speed Stable Region of Magnetically Suspended Rigid Rotors Using Extended Nyquist Criterion and Gain-Stable Region Theory

Wei Jingbo1, Liu Kun1, Gianmarco Radice2

1. College of Aerospace Science and Engineering, National University of Defense Technology, Changsha, China, 410073
2. School of Engineering, University of Glasgow, Glasgow, Scotland, UK, G12 8QQ

**Abstract—This paper presents a novel and simple method to analyze the absolute stability and the rotor speed stable region of a magnetically suspended rotor (MSR). At the beginning of the paper, a complex variable is introduced to describe the movement of the MSR and a complex coefficient transfer function is obtained accordingly. The equivalent stability relationship between this new variable and the two traditional deflection angles is also demonstrated in a simple way. The detailed characteristics of the open-loop MSR system with time delay are studied carefully based on the characteristics of its Nyquist curve. A sufficient and necessary condition of absolute stability is then deduced by using an extended complex Nyquist stability criterion for MSRs. Based on the relationship between the rotor speed and gain-stable region proposed in this paper, the rotor speed stable region can be solved simply and directly. The usefulness and effectiveness of the proposed approaches are validated by examples and simulations.**

**Index Terms—magnetically suspended rotor, complex coefficient transfer function, stability criterion, speed stable region.**

## 1. Introduction

Magnetically suspended rotors (MSRs) have the advantages of non-contact, zero friction, low vibration and dispensing with lubrication. Thus, they can reach high rotating speed and achieve high power storage density. In practice, they are widely used in spacecraft inertial actuators, inertial power storage flywheels, turbo-machineries and industrial spindles [1].

MSRs are multiple-input and multiple-output (MIMO) systems characterized by rotor dynamics, inherently unstable magnetic bearing dynamics and time delay of the controller, which make it difficult to analyze their characteristics and to design proper controllers. In recent decades, many control strategies have been applied to MSRs, such as decentralized PID [2-4], decentralized PID plus cross-feedback [5, 6], centralized PID plus cross-feedback [1, 7-10], adaptive control [11], robust control [12, 13], inverse control [14, 15] and optimal control [16-19]. Among these control methods, centralized PID plus cross-feedback control is widely used in industrial applications because it is simple and convenient to implement.

The stability analysis methods for MSRs are mainly divided into two categories. The first the classical analysis methods in the frequency domain, including the characteristics root method [3, 20-22], Routh-Hurwitz criterion method [4] and root locus method [6]. The characteristics root method is relatively simple; however, it can only analyze the stability at a specified speed. The Routh-Hurwitz criterion method is useful for stability analysis of translation modes, but it can only analyze single-input and single-output (SISO) systems and is not suitable for conical modes. The root locus method is convenient for analyzing the rotor speed stable region, and its main disadvantage is that the stable margins can not be obtained directly. All these methods become difficult when time delay is considered.

The second class of methods is to examine the system by using Lyapunov's theory [14-18, 23]. The Lyapunov's methods can give a perfect mathematical proof of the system stability with a lack of frequency domain information which is very useful in the MSR debugging process.

The complex variable description method is commonly used in the fields of circuit analysis, induction motor, filter design and wireless communication [24]. In that paper, the positive and negative frequency method and some basic characteristics of the complex transfer function are introduced. And in [25], a complex variable is adopted to model an MSR's conical motion. These are insightful works on use of the complex variable description method for MSRs.

In [26-28], positive and negative frequency methods are used to analyze the stability of MSR; however, they can only analyze the stability under a given rotor speed and the stability condition is only necessary and not sufficient. In [21], the speed stable region is obtained by using a critical criterion based on its closed-loop characteristic equation with complex coefficients, however, the calculation is complicated and the relationships between relative stability and stable speed region are not apparently given. The complex coefficient analysis method is extended and applied for a class of cross-coupled anti-symmetrical systems in [7], and is also used to analyze bending modes of MSRs in [29]. The limitations of these works are that the time-delay term should be simplified to a first-order or second-order inertial portion and that it is not convenient to calculate the speed stable region.

This paper attempts to develop a systematical method to analyze the stability analysis of the conical modes of MSRs in the frequency domain. Compared with the existing methods, the proposed method is novel and simple, because the absolute stability and the stable margin can be directly obtained by analyzing the Nyquist curves of MSRs. Meanwhile, the speed stable region can be calculated based on several simple formulations deduced from the proposed gain-stable region theory.

The organization of this paper is as follows. The complex coefficient transfer function of an MSR is deduced in Section 2, as well as the proof of the equivalent relationship between the new complex variable and the two traditional variables. The extended complex Nyquist stability criterion is presented in Section 3 with an example. Section 4 mainly focuses on the characteristics analysis of the open-loop transfer function of the MSR system. The absolute and relative stabilities and the speed stable region, which are the main contributions of this paper, are given in detail and systematically in Section 5 and Section 6. Finally, some conclusions are drawn in Section 7.

## 2. Complex transfer function of MSR

An MSR system usually consists of a rotor, a controller, several magnetic bearings (MBs), and several sensors. Figure 1 shows a common MSR system with the forces generated by the MBs in the *Y*-axis. In the *OYZ* plane, there are two pairs of MBs that provide magnetic forces to suspend the rotor in plane A and plane B. The sensors that measure the displacements of the rotor are in plane C and plane D. The structure of the MSR is symmetric around the *OXY* plane. The distribution of the MBs and the sensors in the *OXZ* plane is the same as those in the *OYZ* plane, so they are not plotted in the figure.

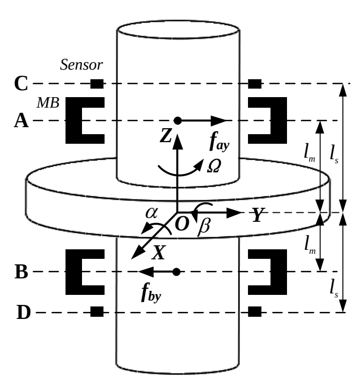


Figure 1. Magnetically suspended rotor system

It is easy to analyze and synthesize the two parallel motions because they are both SISO and decoupled from the conical motions [1]. Thus, the parallel motions are not considered in this paper.

According to the principle of rotor dynamics, the dynamic model of the MSR conical motions is given by

$$\begin{cases} J_r\ddot{\alpha}(t) + J_p\Omega\dot{\beta}(t) = t_\alpha = l_m(f_{ay} - f_{by}) \\ J_r\ddot{\beta}(t) - J_p\Omega\dot{\alpha}(t) = t_\beta = l_m(f_{ax} - f_{bx}) \end{cases} \tag{1}$$

where $m$ is the mass of the rotor, $J_r$ and $J_p$ are the inertial parameters of the rotor, and $\Omega$ is the rotating speed. $x$, $y$ are the parallel displacements of the mass center, and $\alpha$, $\beta$ are the deflection angular displacements around the *X*- and *Y*- axes, respectively. $f_{ax}$, $f_{bx}$, $f_{ay}$, and $f_{by}$ are magnetic forces generated by the corresponding MBs, and they can be transformed into the resultant forces, $f_x$ and $f_y$, on the mass center on the *X*- and *Y*- axes, and the overall torques, $t_\alpha$ and $t_\beta$, on the *Y*- and *X*- axes. $l$ is the distance from the center of the rotor to the plane A.

Suppose that the MBs are identical with each other. The magnetic forces on the rotor can be linearized as follows[1]:

$$f_\upsilon = k_h h_\upsilon + k_i i_\upsilon \quad \upsilon = ax, ay, bx, by, \tag{2}$$

where $h_\upsilon$ is the displacement between the MB and the rotor in the $\upsilon$ channel, and $i_\upsilon$ is the corresponding control current. $k_i$ and $k_h$ denote the force-current coefficient and the force-displacement coefficient of each MB.

As shown in Figure 1, the deflection angles can be calculated by (3) from the displacements, $h_{cx}$, $h_{cy}$, $h_{dx}$ and $h_{dy}$, which are measured by the sensors.

$$\begin{cases} \alpha = (h_{cy} - h_{dy})/2l_s \\ \beta = (h_{cx} - h_{dx})/2l_s \end{cases}. \tag{3}$$

Substituting (2) into (1) yields

$$\begin{cases} J_r\ddot{\alpha}(t) + J_p\Omega\dot{\beta}(t) - 2k_h l_m^2\alpha(t) = 2k_i l_m i_\alpha(t) \\ J_r\ddot{\beta}(t) - J_p\Omega\dot{\alpha}(t) - 2k_h l_m^2\beta(t) = 2k_i l_m i_\beta(t) \end{cases}, \tag{4}$$

where, the control currents, $i_\alpha(t)$ and $i_\beta(t)$, are defined by

$$\begin{cases} i_\alpha(t) = [i_{ay}(t) - i_{by}(t)]/2 \\ i_\beta(t) = [i_{ax}(t) - i_{bx}(t)]/2 \end{cases}. \tag{5}$$

Then, the Laplace transformation of (4) is given by

$$\begin{cases} J_r\alpha(s)s^2 + J_p\Omega\beta(s)s - 2k_h l_m^2\alpha(s) = 2k_i l_m i_\alpha(s) \\ J_r\beta(s)s^2 - J_p\Omega\alpha(s)s - 2k_h l_m^2\beta(s) = 2k_i l_m i_\beta(s) \end{cases}. \tag{6}$$

The decoupled and centralized PID plus cross-feedback control law is widely used for MSRs. As a special portion added to a common PID control law, the cross-feedback term is employed to suppress the gyro effects [7, 9, 28]. As shown in (7), the inputs of the controller are the angles, $\alpha_m$ and $\beta_m$, while the outputs of the controller are the desired current commands, $i_\alpha^*$ and $i_\beta^*$.

$$
\begin{cases}
i_\alpha^*(t) = -[\underbrace{k_P\alpha_m(t-\tau) + k_I\int\alpha_m(t-\tau)dt + k_D\dot{\alpha}_m(t-\tau)}_{g_b(\alpha_m(t-\tau))} - \underbrace{k_C\dot{\beta}_m(t-\tau)}_{g_{cr}(\beta_m(t-\tau))}] \\
i_\beta^*(t) = -[\underbrace{k_P\beta_m(t-\tau) + k_I\int\beta_m(t-\tau)dt + k_D\dot{\beta}_m(t-\tau)}_{g_b(\beta_m(t-\tau))} + \underbrace{k_C\dot{\alpha}_m(t-\tau)}_{g_{cr}(\alpha_m(t-\tau))}]
\end{cases}, \quad (7)
$$

where, $k_P$, $k_I$ and $k_D$ are the proportional, integral and differential coefficients, respectively, $k_C$ is the cross-feedback coefficient, and $\tau$ is the time delay of the controller which is usually caused by the calculation time in the physical digital controller. $g_b(\cdot)$ and $g_{cr}(\cdot)$ denote the common PID portion and the cross-feedback portion, respectively.

The control parameters are usually determined by engineering experience, but some simple principles can be followed. The proportional coefficient $k_P$ is usually selected to make the stiffness of the closed-loop system approximately equal the force-displacement coefficient $k_h$, which can give a "natural" stiffness for the closed-loop system to suppress uncertainties. Then the choice of the differential coefficient $k_D$ is subject to the closed-loop stiffness, which should be high enough to provide enough oscillation attenuation and not too high to avoid a high noise level [1]. The integral coefficient $k_I$ is usually very small and relatively easy to determine. The cross-feedback coefficient $k_C$ is very useful to achieve a high rotating speed of the rotor and can be neglected in the low speed range, which can be demonstrated in the simulation in Section 5, where $k_C = 0$.

Then, the Laplace transformation of (7) is given by

$$
\begin{cases}
i_\alpha^*(s) = -[G_b(s)\alpha_m(s) - G_{cr}(s)\beta_m(s)]e^{-\tau s} \\
i_\beta^*(s) = -[G_b(s)\beta_m(s) + G_{cr}(s)\alpha_m(s)]e^{-\tau s}
\end{cases}. \quad (8)
$$

where, $G_b(s) = k_P + k_I\dfrac{1}{s} + k_D s$ and $G_{cr}(s) = k_C$.

The transfer functions of the sensor, the power amplifier and the low-pass filter should also be considered in the closed-loop control system. They are defined as $k_s$, $G_a(s)$ and $G_f(s)$, respectively. $k_s$ is a scale parameter, while $G_a(s)$ and $G_f(s)$ are given by

$$
\begin{cases}
G_a(s) = \dfrac{1}{\tau_a s + 1} \\
G_f(s) = \dfrac{1}{(\tau_f s + 1)^2}
\end{cases}, \quad (9)
$$

where, $\tau_a$ is the time constant of $G_a(s)$ and $\tau_f$ is the low-pass filter coefficient of $G_f(s)$, respectively.

The final closed-loop control system is shown as the block diagram in Figure 2.

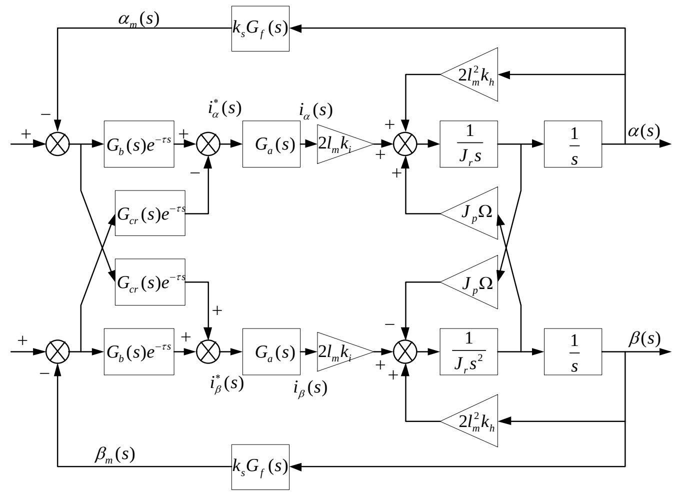


Figure 2. Block diagram of MSR control system

From the block diagram and equations (6)~(8), the closed-loop model is given by

$$
\begin{cases}
J_r\alpha(s)s^2 + J_p\Omega\beta(s)s - 2k_hl_m^2\alpha(s) \\
\qquad = 2k_ik_sl_mG_a(s)G_f(s)[G_b(s)\alpha(s) - G_{cr}(s)\beta(s)]e^{-\tau s} \\
J_r\beta(s)s^2 - J_p\Omega\alpha(s)s - 2k_hl_m^2\beta(s) \\
\qquad = 2k_ik_sl_mG_a(s)G_f(s)[G_b(s)\beta(s) + G_{cr}(s)\alpha(s)]e^{-\tau s}
\end{cases}. \quad (10)
$$

Define $\varphi(t) = \alpha(t) + j\beta(t)$, where $j = \sqrt{-1}$. The convergence characteristics of $\varphi$ and those of $\alpha$ and $\beta$ are equivalent, which can be proved as follows.

**a.** If $\varphi$ is asymptotically stable, then $\alpha$ and $\beta$ are also asymptotically stable.

If $\varphi$ is asymptotically stable, it is also exponentially stable because the system (10) is linear if neglecting time delay. Thus, a positive constant $\varepsilon$ exists so that $|\varphi(t)| \le |\varphi(0)|e^{-\varepsilon t}$. Then, the relationship (11) holds, where $\lambda = \max(\varphi(0)/\alpha(0), \varphi(0)/\beta(0))$. So, $\alpha$ and $\beta$ are asymptotically stable.

$$
\begin{cases}
|\alpha(t)| \le \sqrt{\alpha(t)^2 + \beta(t)^2} = |\varphi(t)| \le |\varphi(0)|e^{-\varepsilon t} \le \lambda|\alpha(0)|e^{-\varepsilon t} \\
|\beta(t)| \le \sqrt{\alpha(t)^2 + \beta(t)^2} = |\varphi(t)| \le |\varphi(0)|e^{-\varepsilon t} \le \lambda|\beta(0)|e^{-\varepsilon t}
\end{cases}. \quad (11)
$$

b. If $\alpha$ and $\beta$ are asymptotically stable, then $\varphi$ is also asymptotically stable.

If $\alpha$ and $\beta$ are asymptotically stable, they are also exponentially stable because the system (10) is linear if neglecting time delay. Thus, two positive constants $\varepsilon_1$, $\varepsilon_2$ exist, so that $|\alpha(t)| \le |\alpha(0)|e^{-\varepsilon_1 t}$ and $|\beta(t)| \le |\beta(0)|e^{-\varepsilon_2 t}$. Then, the relationship (12) holds, where $\varepsilon = \min(\varepsilon_1, \varepsilon_2)$. So, $\varphi$ is asymptotically stable.

$$
\begin{aligned}
|\varphi(t)| &= \sqrt{\alpha(t)^2 + \beta(t)^2} \le \sqrt{\left(|\alpha(0)|e^{-\varepsilon_1 t}\right)^2 + \left(|\beta(0)|e^{-\varepsilon_2 t}\right)^2} \\
&\le \sqrt{\left(|\alpha(0)|\right)^2 + \left(|\beta(0)|\right)^2}\,e^{-\varepsilon t} = |\varphi(0)|e^{-\varepsilon t}
\end{aligned}. \quad (12)
$$

The Laplace transform of $\varphi(t)$ is given by $\varphi(s) = \alpha(s) + j\beta(s)$. Then Eq. (10) can be reformulated as (13) with the complex variable $\varphi(s)$. Similarly, Figure 2 can be transformed into Figure 3.

$$\begin{aligned} &J_r\varphi(s)s^2 - jJ_p\Omega\varphi(s)s - 2k_h l_m^2\varphi(s) \\ &= -2l_m k_i k_s G_a(s)G_f(s)[G_b(s) + jG_{cr}(s)]\varphi(s)e^{-\tau s} \end{aligned} . \tag{13}$$

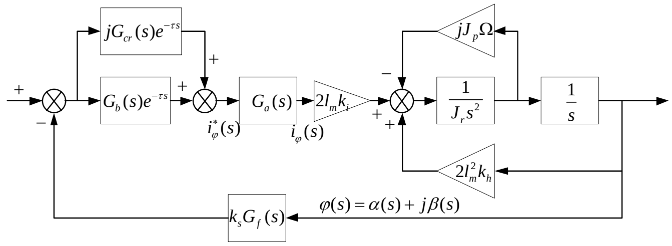


Figure 3. Block diagram of MSR control system with complex variable

Then, the model of the MSR is given by

$$P(s) = \frac{2l_m k_i}{J_r s^2 - jJ_p\Omega s - 2k_h l_m{}^2} . \tag{14}$$

The transfer function of the whole controller, whose inputs are the complex deflection angles and whose outputs are the currents in the coils of the MBs, is given by

$$C(s) = k_s G_f(s)G_a(s)[G_b(s) + jG_{cr}(s)]e^{-\tau s} . \tag{15}$$

The open-loop complex coefficient transfer function can be obtained as

$$\begin{aligned} &G_{open}(s) = C(s)P(s) \\ &= k_s G_a(s)G_f(s)[G_b(s) + jG_{cr}(s)]e^{-\tau s}\frac{2l_m k_i}{J_r s^2 - jJ_p\Omega s - 2k_h l_m{}^2} \end{aligned} , \tag{16}$$

where, $e(s)$ is the error between the required angles and the real ones. Here, the rotor is expected to be suspended at the equilibrium position, so the desired angles are both zero.

## 3. Nyquist criterion for complex coefficient transfer functions with time delay

Since there are several complex coefficients in the open-loop transfer function of the MSR, it is necessary to discuss whether the Nyquist criterion, which is always used in real coefficient transfer functions, can be directly used.

For a real coefficient polynomial, the complex roots are known to arise in pairs and are also conjugated. However, a single complex root can solely arise in a complex coefficient polynomial. Thus, for complex coefficient transfer functions, the symmetrical nature of the roots around the real axis in the complex plane no longer holds true [24]. As a result, the Nyquist curve should be plotted completely in the whole frequency region from $-\infty$ to $+\infty$. An example is given below to show the asymmetry of the roots of a complex coefficient polynomial.

***Example 1***: $G(s) = s + a + bj$ , $a, b \in \mathrm{R}$ , $b \neq 0$ .

Since $\mathrm{Im}[G(j\omega)] = \mathrm{Im}(j\omega + a + bj) = b + \omega$ , and $\mathrm{Im}[G(-j\omega)] = \mathrm{Im}(-j\omega + a + bj) = b - \omega$ , $\forall \omega \in (-\infty, \infty)$ , then, $\mathrm{Im}[G(j\omega)] \neq \mathrm{Im}[G(-j\omega)]$ . If $a = 2$ and $b = 8$ , when $\omega = 2$ , $\mathrm{Im}[G(2j)] = 10$ ; however, $\mathrm{Im}[G(-2j)] = -6$ .

### *3.1. Extended Nyquist criterion*

***Theorem 1 (Nyquist Stability Criterion for Complex Coefficient Transfer Functions)*:** As for a real transfer function with *complex coefficients* and *time delay*, there are $P$ poles on the right-half plane. The sufficient and necessary condition for the absolute stability of its closed-loop transfer function is that its Nyquist curve encircles (-1, j0) counter-clockwise $P$ times for $s = j\omega$ , $-\infty < \omega < \infty$ .

***Proof*:** The real transfer function with *complex coefficients* and *time-delay* is meromorphic, according to *Cauchy's argument principle*, the number of poles of the closed-loop transfer function in the right-half plane equals the number of poles of the open-loop transfer function in the right-half plane minus the number of its Nyquist curve encircles (-1, j0) counter-clockwise. When they are equal, the closed-loop transfer function has no pole on the right-half complex plane and the system is absolutely stable.

The transfer functions of physical systems are always strictly real, that is, the order of the numerator m is always smaller than that of the denominator n (m<n). Because the gain is always zero on the domain of $s = \infty\vartheta$ , $-90^\circ < \vartheta < 90^\circ$ , the phase value will be meaningless. Thus, only the domain of $s = j\omega$ $(-\infty < \omega < \infty)$ is considered in this paper.

***Remark 1*:** Since the Nyquist curve is not always symmetric around the real axis, the gain-frequency curve and the phase-frequency curve are also not always symmetric around the imaginary axis $\omega = 0$ . Thus, they must be plotted fully in all frequency regions from $-\infty$ to $+\infty$ in the Bode diagram.

***Corollary 1*:** For the complex coefficient transfer function with time-delay and if there are $P$ poles on the right-half plane, the sufficient and necessary condition for the absolute stability of its closed-loop function is that its phase-frequency curve positively crosses the lines that $\varphi = (2k+1)\pi$ ( $k = \pm 1, \pm 2, \pm 3 \cdots$ ) for $P$ times in the frequency region $A(\omega) = |G(j\omega)| > 1$ .

According to the geometrical relationships among the gain-frequency curve, phase-frequency curve and Nyquist curve, *Corollary 1* can be easily deduced from *Theorem 1*.

***Remark 2*:** The definition of a positive crossing is that the Nyquist curve crosses the lines that $\varphi = (2k+1)\pi$ ( $k = \pm 1, \pm 2, \pm 3 \cdots$ ) from bottom to top when $\omega$ increases. So the negative crossing is from top to bottom when $\omega$ increases. This definition is more simple and distinct than that in [21, 27]. It is important to note that $\omega$ increases from $-\infty$ to $+\infty$ .

### *3.2. Relative stability*

For transfer functions with real coefficients, when the system is absolutely stable, the relative stabilities can be obtained based on the Nyquist curve, or based on the gain-frequency curve and the phase-frequency curve. They are often described by stability margins, including gain margin and phase margin. For complex coefficient transfer functions, the stability margins are redefined as the gain-stable region and the phase-stable region in this paper.

***Gain-Stable Region***

Suppose that there are $\kappa$ intersection points of a Nyquist curve and the negative real axis, denoted as $L_1$ , $L_2$ , …, $L_\kappa$ .

Among these points, $L_1$ is the nearest one to (-1, j0) outside the unit circle and $L_2$ is the nearest one to (-1, j0) inside the unit circle. As shown in Figure 4, $l_1$ and $l_2$ are the distances from $L_1$ and $L_2$ to (-1, j0), respectively. Afterwards, the gain-stable condition is $1/l_1 < h < 1/l_2$ which means that the system will be unstable if the gain of the open-loop function increases by $1/l_2$ times or decreases by $1/l_1$ times.

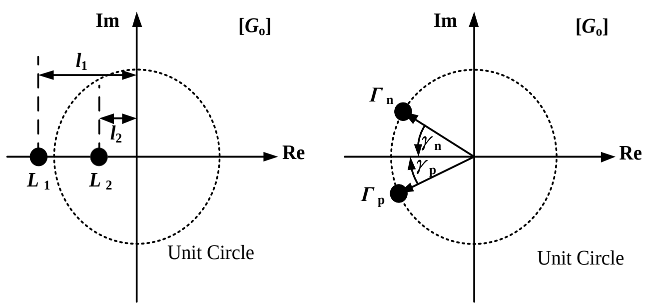


Figure 4. Relative stabilities

***Phase-Stable Region***

Suppose that there are $\lambda$ intersections points of the Nyquist curve and the unit circle, denoted as $\Gamma_1$, $\Gamma_2$, …, $\Gamma_m$. $\Gamma_p$ is the nearest one to (-1, j0) in the positive frequency segments below the negative real axis, and $\Gamma_n$ is the nearest one to (-1, j0) in the negative frequency segments above the negative real axis. As shown in Figure 4, $\gamma_p$ and $\gamma_n$ are the absolute angles from $\Gamma_p$ and $\Gamma_n$ to the negative real axis, respectively. Moreover, $\omega_p$ and $\omega_n$ are the frequencies at $\Gamma_p$ and $\Gamma_n$, respectively. Afterwards, the phase-stable region is defined as: $\gamma_p$ at $\omega_p$ and $\gamma_n$ at $\omega_n$, which means the system will be unstable if the phase angle is delayed by $\gamma_p$ at $\omega_p$ or delayed by $\gamma_n$ at the frequency $\omega_n$.

Furthermore, the time-delay margin also can be solved by

$$\tau_c = \min(\gamma_n / |\omega_n|, \gamma_p / \omega_p), \tag{17}$$

which means that the system will lose stability if the time delay increases by $\tau_c$.

***Remark 4***: The definitions of the gain-stable region and the phase-stable region are very useful for designing a proper controller, selecting controller parameters and solving the stable region of variable parameters. For example, when there is a variable parameter in the transfer function, to ensure stability, some inequality constraints with this parameter will hold to meet the gain-stable and the phase-stable conditions. Then, it will be very convenient to solve the stable region of this parameter. This method will be used for solving the speed stable region of MSRs.

### *3.3. Example 2*

An example is employed to demonstrate the proposed theories. The example system is given by

$$\begin{cases} \ddot{\xi}(t) + 3\dot{\zeta}(t) - 2\xi(t) = u_\xi \\ \ddot{\zeta}(t) - 3\dot{\xi}(t) - 2\zeta(t) = u_\zeta \end{cases}. \tag{18}$$

Suppose the control law is PID plus cross-feedback control, the cross-feedback coefficient is not accurate with a bias and the time delay is $\tau = 0.1$ in the controller. The whole controller is formulated as

$$\begin{cases} u_\xi = -4\xi(t-\tau) - 2\dot{\xi}(t-\tau) - 0.1\int \xi(t-\tau)dt + 2.8\dot{\zeta}(t-\tau) \\ u_\zeta = -4\zeta(t-\tau) - 2\dot{\zeta}(t-\tau) - 0.1\int \zeta(t-\tau)dt - 2.8\dot{\xi}(t-\tau) \end{cases} \tag{19}$$

Define $\eta(t) = \xi(t) + j\zeta(t)$, $\upsilon = u_\xi + ju_\zeta$, then, the system is converted into (20).

$$\begin{cases} \ddot{\eta}(t) - j3\dot{\eta}(t) - 2\eta(t) = \upsilon \\ \upsilon = -4\eta(t-\tau) - (2+2.8j)\dot{\eta}(t-\tau) - 0.1\int \eta(t-\tau)dt \end{cases}. \tag{20}$$

Suppose the system has a unit negative feedback loop. By conducting a Laplace transform for (20), the transfer functions of the plant and the controller are given by

$$\begin{cases} P'(s) = \dfrac{1}{s^2 - j3s - 2} \\ C'(s) = [4 + (2+2.8j)s + \dfrac{0.1}{s}]e^{-0.1s} \end{cases}. \tag{21}$$

Thus, the open-loop transfer function is

$$\begin{aligned} G_o'(s) &= C'(s)P'(s) = [4 + (2+2.8j)s + \frac{0.1}{s}]\frac{1}{s^2 - j3s - 2}e^{-0.1s} \\ &= \frac{(2+2.8j)s^2 + 4s + 0.1}{s(s^2 - j3s - 2)}e^{-0.1s} \end{aligned}. \tag{22}$$

The Nyquist curve of $G_o'(s)$ is given as Figure 5. As shown in the figure, the Nyquist curve of $G_o'(s)$ encircles (-1, j0) counter-clockwise for zero time. Thus, there is no unstable pole in the closed-loop system and the system is stable. From the Nyquist curve in Figure 5, $l_1 = 1.66$ and $l_2 = 0.49$. Based on the gain- and phase-stable theories, the gain- and phase-stable regions of the system (22) are approximately given by: $2.04 > h > 0.60$, $\gamma_p = 104.2^\circ$ at $\omega_p = 5.58$ and $\gamma_n = 10.4^\circ$ at $\omega_n = 1.57$.

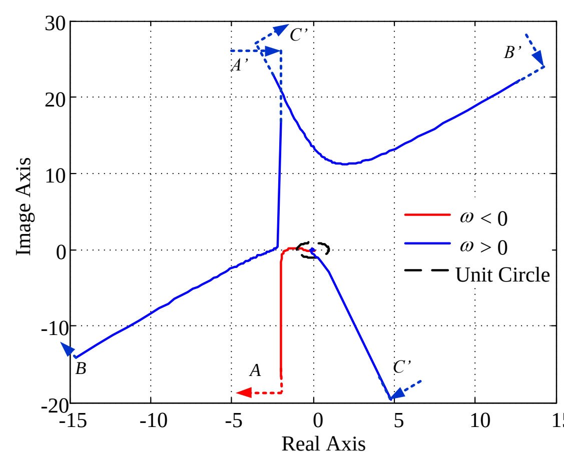


(a)

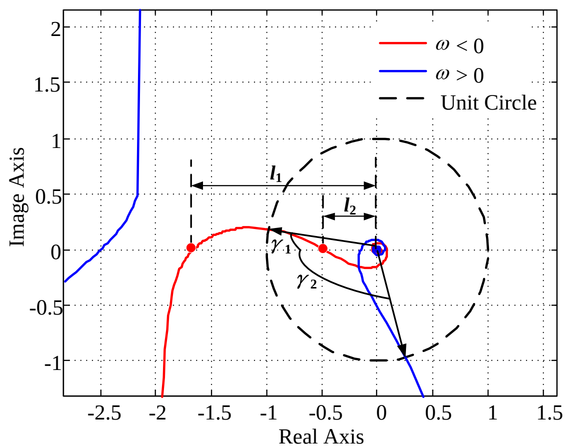


(b)

Figure 5. Global (a) and local (b) plots of Nyquist curve of $G'_o(s)$ .are a global plot and a local plot, respectively. There are three clockwise infinite semi-circles not plotted in the figure (a), they are arcs from A to A′, B to B′, and C to C′.

To evaluate the influences of the time delay on the system, the gain and phase of the time-delay portion are calculated by

$$\begin{cases} \left| e^{-j\omega\tau} \right| = 1 \\ \angle e^{-j\omega\tau} = -\omega\tau \end{cases}. \tag{23}$$

Define $G''_o(s)$ as the transfer function of the system (22) without the time-delay portion, the gain and phase frequency functions of the original transfer function $G'_o(s)$ are given by

$$\begin{cases} \left| G'_o(j\omega) \right| = \left| G''_o(j\omega) \right| \\ \angle G'_o(j\omega) = \angle G''_o(j\omega) - \tau\omega \end{cases}. \tag{24}$$

Since the gain of the time-delay portion always equals one regardless of the value of the time-delay, the time-delay will only affect the phase lag. From the second equitation of (24), the larger the time delay is, the larger the phase lag is. As for the Nyquist curve, the positive segment will turn clockwise (counter-clockwise) and the negative will turn counter-clockwise (clockwise) if the time delay increases (decreases). To illustrate the phenomenon, Figure 6 is plotted to show the Nyquist curve of the system (22) when $\tau = 0.2$ . Meanwhile, the time-delay margin can be calculated by (17), that is $\tau_c = 0.12$ .

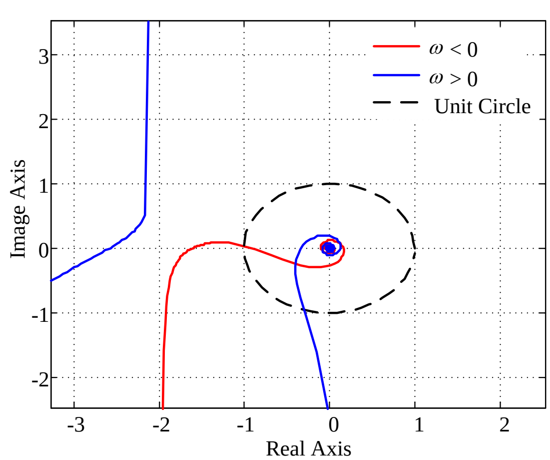


Figure 6. Nyquist curve of $G'_o$ when $\tau = 0.2$

As shown in Figure 6 and compared with Figure 5, the segments (blue lines) of the Nyquist curve in the positive frequency region have rotated clockwise, and the ones (red lines) in the negative frequency region have rotated counter-clockwise.

Based on the definition of the phase-stable region and the above analysis, it is concluded that the time delay will minimize phase-stable region and make the stability of a stable system weak. However, the influence on the gain-stable region is uncertain because there is no certain relationship between gain-stable region and time delay. In this example, the gain-stable region also shrinks.

## 4. Characteristics of open-loop MRS system

During the working period in the MSR system, rotor speed is a variable parameter, which is a difference from example 2. The transfer function will change if the rotor speed changes. To conveniently study the MSR stability problem, the detailed characteristics of the open-loop MSR system should be previously analyzed.

### *4.1. Unstable poles and poles on the imaginary axis*

The unstable poles of $G_{open}(s)$ will be those in the MSR plant $P(s)$ because there is no unstable pole in the controller $C(s)$ .

Define $f(s) = J_r s^2 - jJ_p\Omega s - 2k_h l_m^{\ 2}$ which is the denominator portion of $P(s)$ in (14). The roots of the equation, $f(s) = 0$ , are:

$$s_1 = \frac{jJ_p\Omega + \sqrt{\Delta}}{2J_r}, \quad s_2 = \frac{jJ_p\Omega - \sqrt{\Delta}}{2J_r}, \tag{25}$$

where $\Delta = 8J_r k_h l_m^{\ 2} - (J_p\Omega)^2$ . Then, the number of the unstable poles is discussed in two cases as in Table 1.

Table 1. Unstable pole Number of $G_{open}(s)$

| | |
|---|---|
| Case A: $\lvert\Omega\rvert < \Omega_c$ , $\Delta > 0$ | 1 unstable pole. |
| Case B: $\lvert\Omega\rvert \geq \Omega_c$ , $\Delta \leq 0$ | 0 unstable pole. |

Before analyzing the curve shape of $G_{open}(j\omega)$ in the complex plane, the poles on the imaginary axis should be examined. There is one pole at the original point of the complex plane for both cases because of the integral part of the PID plus cross-feedback controller. The distribution of poles on the imaginary axis of $P(s)$ should also be discussed in the two cases as in Table 2.

Table 2. Pole number on imaginary axis of $G_{open}(s)$

| | |
|---|---|
| Case A: $\lvert\Omega\rvert < \Omega_c$ | $s_1 = j0$ . |
| Case B: $\lvert\Omega\rvert \geq \Omega_c$ | $s_1 = j0$ , $s_2 = j\omega_{C2}$ , $s_3 = j\omega_{C3}$ . |

where $\Omega_c = \sqrt{8J_r k_h l_m^{\ 2}} / J_p$ . $\omega_{C2}$ and $\omega_{C3}$ are given by (26), and they can be obtained by solving the equation $\mathrm{Re}[f(j\omega)] = 0$ . It is easy to find that the sum of $\omega_{C2}$ and $\omega_{C3}$ is $J_p\Omega / J_r$ from (26).

$$\omega_{C2} = \frac{1}{2}\frac{J_p}{J_r}\left(\Omega + \sqrt{\Omega^2 - \Omega_c^{\ 2}}\right),\ \omega_{C3} = \frac{1}{2}\frac{J_p}{J_r}\left(\Omega - \sqrt{\Omega^2 - \Omega_c^{\ 2}}\right). \quad (26)$$

### 4.2. Characteristics of $G_{open}(j\omega)$ on the Complex Plane

Substituting $s = j\omega$ into (16), the open-loop frequency response function is given by

$$G_{open}(j\omega) = k_s G_a(j\omega)[G_b(j\omega) + jG_{cr}(j\omega)]G_f(j\omega)e^{-\tau j\omega} \times \frac{2l_m k_i}{-J_r\omega^2 + J_p\Omega\omega - 2k_h l_m^{\ 2}}. \quad (27)$$

Table 3. Number of Infinite Semi-Circles

| | |
|---|---|
| Case A: $\lvert\Omega\rvert < \Omega_c$ | 1 at $\omega = 0$. |
| Case B: $\lvert\Omega\rvert \geq \Omega_c$ | 3 at $\omega = 0$, $\omega_{C2}$, $\omega_{C3}$. |

According to the plotting principles of Nyquist curves, it will turn 180° clockwise with an infinite radius once if there is one pole on the imaginary axis. The number of poles on the imaginary axis changes for different rotor speeds, and the Nyquist curves will have different shapes accordingly. The number of infinite semi-circles of the system is given in Table 3.

### 4.3. Relationships between $\angle G_{open}(j\omega)$ and $C(j\omega)$, $P(j\omega)$

The frequency response functions of the MSR and the controller are given by

$$\begin{cases} P(j\omega) = \dfrac{2l_m k_i}{-J_r\omega^2 + J_p\Omega\omega - 2k_h l_m^{\ 2}} \\ C(j\omega) = k_s G_a(j\omega)[G_b(j\omega) + jG_{cr}(j\omega)]e^{-\tau j\omega}G_f(j\omega) \end{cases}. \quad (28)$$

Thus, the gain-frequency function and the phase-frequency function can be obtained as in (29) accordingly.

Note that $P(j\omega)$ is real when $\omega$ increases from $-\infty$ to $\infty$. Thus, $P(j\omega)$ is a real function about frequency and rotor speed, which can be formulated as $P(\omega,\Omega)$. The phase-frequency function $\angle G_{open}(j\omega)$ of $G_{open}(j\omega)$ will vary with rotor speed, which is given by Table 4.

From the aforementioned analysis, the characteristics of the phase-frequency function are completely determined by the controller $C(s)$ when the rotor speed is given.

***Remark 4***: There are one (three) infinite-semi circle(s) when the absolute value of the rotor speed is below (above) $\Omega_c$. The rotor speed will only change the gain of the open-loop transfer function, because the controller does not contain any term about the rotor speed, which makes it possible to solve the speed stable region by using the proposed gain-stable region in Section 3.

Table 4. Phase Characteristics of $G_{open}(j\omega)$

| | | |
|---|---|---|
| Case A: $\lvert\Omega\rvert < \Omega_c$ | | $\angle P(j\omega) = -180^\circ$, $\angle G_{open}(j\omega) = \angle C(j\omega) - 180^\circ$ |
| Case B: $\lvert\Omega\rvert \geq \Omega_c$ | $\omega \in (-\infty, \omega_{C2})$ | $\angle P(j\omega) = -180^\circ$ $\angle G_{open}(j\omega) = \angle C(j\omega) - 180^\circ$ |
| | $\omega \in (\omega_{C2}, \omega_{C3})$ | $\angle P(j\omega) = -360^\circ$ $\angle G_{open}(j\omega) = \angle C(j\omega) - 360^\circ$ |
| | $\omega \in (\omega_{C3}, +\infty)$ | $\angle P(j\omega) = -540^\circ$ $\angle G_{open}(j\omega) = \angle C(j\omega) - 540^\circ$ |

$$\begin{cases} \left|G_{open}(j\omega)\right| = \left|k_s G_a(j\omega)[G_b(j\omega) + jG_{cr}(j\omega)]e^{-\tau j\omega}G_f(j\omega)\right|\left|\dfrac{2l_m k_i}{-J_r\omega^2 + J_p\Omega\omega - 2k_h l_m^{\ 2}}\right| = \left|C(j\omega)\right|\left|P(j\omega)\right| = \left|C(j\omega)\right|\left|P(\omega,\Omega)\right| \\ \angle G_{open}(j\omega) = \angle\left\{k_s G_a(j\omega)[G_b(j\omega) + jG_{cr}(j\omega)]e^{-\tau j\omega}G_f(j\omega)\dfrac{2l_m k_i}{-J_r\omega^2 + J_p\Omega\omega - 2k_h l_m^{\ 2}}\right\} = \angle C(j\omega) + \angle P(\omega,\Omega) \end{cases} \quad (29)$$

## 5. Stability criterion of the MSR

### 5.1. Stability criterion of the MSR

According to the Nyquist stability criterion for complex coefficient transfer functions in Section 3 and the analysis in Section 4, a stability criterion under a given rotor speed can be concluded as Theorem 2.

***Theorem 2 (Stability Criterion of MSR)***: the sufficient and necessary condition for the absolute stability of an MSR utilizing PID plus cross-feedback controller, is that its open-loop Nyquist curve encircles (-1, j0) counter-clockwise once if $\lvert\Omega\rvert < \Omega_c$ and zero times if $\lvert\Omega\rvert \geq \Omega_c$.

### 5.2. Example 3

The parameters of an MSR are given in Table 5. Thus, $\Omega_c$ can be obtained as

$$\Omega_c = \sqrt{8J_r k_h l_m^{\ 2}} \big/ J_p = 7988.6\text{rpm}. \quad (30)$$

The Nyquist curve when the rotor speed is 3000 rpm is shown in Figure 7, and that of 12000 rpm is shown in Figure 8.

In Figure 7, there is only one infinite semi-circle at frequency $\omega = 0$ rad/s, while in Figure 8 there are three infinite semi-circles at the frequencies $\omega = 0$ rad/s, 177.2rad/s, and 1219.1rad/s, which validates the analysis in Section 4. According to the relationships between the Bode diagram and the Nyquist curve, the phase-frequency curve of the Bode diagram will turn 180° for once at $\omega = 0$ rad/s and thrice at $\omega = 0$ rad/s, 177.2 rad/s, and 1219.1 rad/s in the whole frequency region in this case. This phenomenon can also be found in [21, 26, 27].

Table 5. System and control parameters of an MSR

| Parameters | Values | Parameters | Values |
|---|---|---|---|
| $J_p$ | 1.0 kg·m² | $k_a$ | 4.8 A/V |

| | | | |
|---|---|---|---|
| $k_h$ | 3 N/μm | $k_P$ | 0.2 |
| $J_r$ | 0.9 kg·m$^2$ | $k_C$ | 0.0 |
| $k_s$ | 8000 V/μm | $k_I$ | 1.7 |
| $k_i$ | 1350 N/A | $k_D$ | 0.0008 |
| $l_m$ | 0.24 m | $\tau$ | 0.00013 s |
| $\tau_f$ | $3.3\times10^{-5}$ | $\tau_a$ | 0.0005 |

***Absolute stability***: When $\Omega = 3000\text{rpm}$, the open-loop transfer function has one unstable pole on the right half-plane, namely $P=1$. Its Nyquist curve encircles (-1, j0) once, thus $N=1$. The number of unstable poles of the closed-loop system is $Z=P-N=0$, so the system is stable. When $\Omega = 12000\text{rpm}$, $P=0$ and $N=0$, so $Z=P-N=0$ and the closed-loop system is also stable.

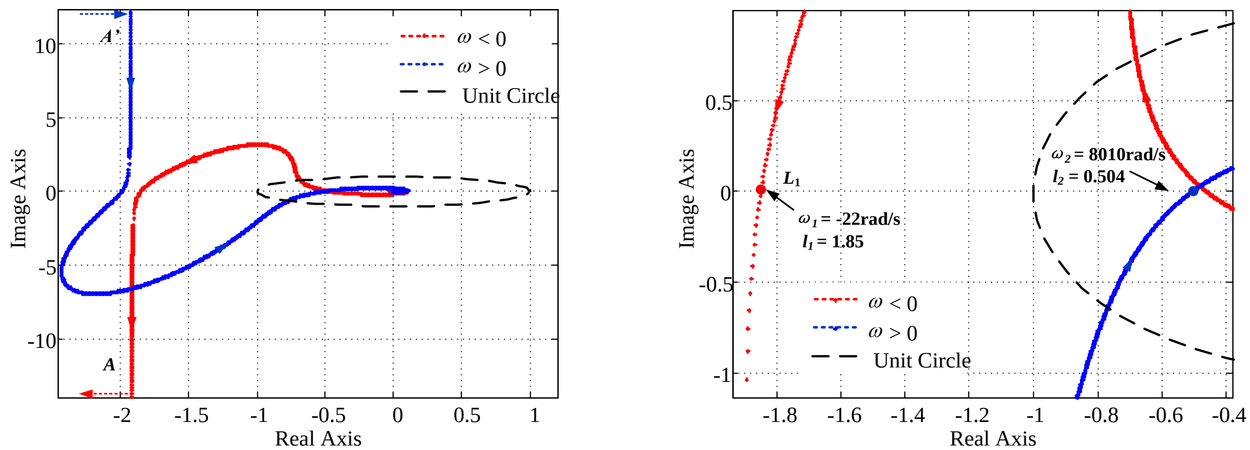


Figure 7. Global (left) and local (right) plots of Nyquist curve when $\Omega = 3000\text{rpm}$. The Nyquist curve begins from the original point at $\omega = -\infty$, reaches infinite point A along the red line, turns 180° clockwise from A to A′, then comes back to the original point along the blue line. The direction is shown by arrows.

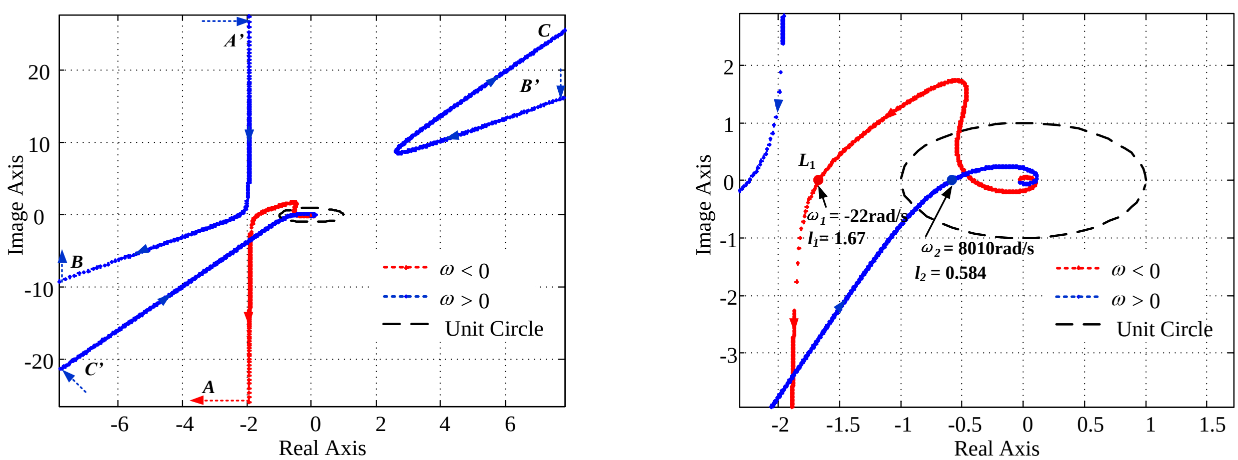


Figure 8. Global (left) and local (right) plots of Nyquist curve when $\Omega = 12000\text{rpm}$. The Nyquist curve begins from the original point at $\omega = -\infty$, reaches infinite point A along the red line, and turns 180° clockwise from A to A′, from B to B′ and from C to C. Finally, comes back to the original point along the blue line. The direction is shown by arrows.

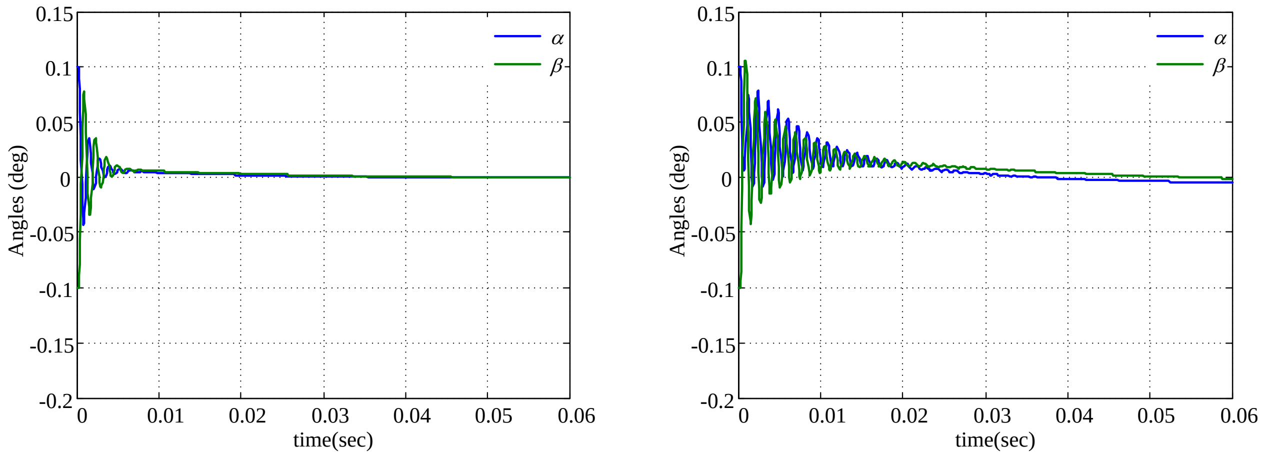


Figure 9. Simulation results at 3000 rpm (left`) and 12000 rpm (right). The initial condition is: $\alpha = 0.1^{\circ}$, $\beta = -0.1^{\circ}$.

***Relative Stability***: Figure 7 shows that at $\Omega = 3000\text{rpm}$, the nearest points inside and outside the unit circle are $L_1$ and $L_2$ respectively, thus, the gain-stability region is $(0.5405, 1.9841)$. And when $\Omega = 12000\text{rpm}$, the gain-stable region is $(0.5988, 1.7123)$ in Figure 8. The simulation results in the time domain at different rotor speeds are shown in Figure 9.

## 6. Speed stable region

### 6.1. Methods

In Section 4, it is concluded that the varying rotor speed will only change the gain of the open-loop transfer function. In other words, rotor speed will not change the crossing frequencies of the intersection points of the Nyquist curve and the negative real axis.

Suppose the rotor speed is positive. The case of the negative rotor speed will be symmetric with that of the positive one.

Define $g(\omega,\Omega) = J_r\omega^2 - J_p\Omega\omega + 2k_h l_m{}^2$. The ratio of the gains in two different speeds at a certain frequency can be given by

$$\frac{l_{\Omega_1,L_i}}{l_{\Omega_2,L_i}} = \frac{|G(j\omega_i)|_{\Omega_1}}{|G(j\omega_i)|_{\Omega_2}} = \left|\frac{\left(-J_r\omega_i^2 + J_p\Omega_2\omega_i - 2k_h l_m{}^2\right)}{\left(-J_r\omega_i^2 + J_p\Omega_1\omega_i - 2k_h l_m{}^2\right)}\right| = \frac{|g(\omega_i,\Omega_2)|}{|g(\omega_i,\Omega_1)|} \tag{31}$$

The equations below can be obtained from (29).

$$|C(j\omega)| = \frac{|G(j\omega,\Omega)|}{|P(\omega,\Omega)|} = \frac{l_\Omega}{|P(\omega,\Omega)|}, \tag{32}$$

$$\begin{cases} |G(j\omega_1,\Omega)| > 1 \\ |G(j\omega_2,\Omega)| < 1 \end{cases}, \tag{33}$$

where $\omega_1$ and $\omega_2$ are the frequencies at points $L_1$ and $L_2$, respectively. Namely,

$$\begin{cases} \dfrac{l_{\Omega_1,L_1}}{|P(\omega_1,\Omega_1)|}|P(\omega_1,\Omega)| = \dfrac{|g(\omega_1,\Omega_1)|}{|g(\omega_1,\Omega)|} l_{\Omega_1,L_1} > 1 \\ \dfrac{l_{\Omega_1,L_2}}{|P(\omega_2,\Omega_1)|}|P(\omega_2,\Omega)| = \dfrac{|g(\omega_2,\Omega_1)|}{|g(\omega_2,\Omega)|} l_{\Omega_1,L_2} < 1 \end{cases}. \tag{34}$$

Hence, the rotor speed stable region is determined by

$$\begin{cases} |g(\omega_1,\Omega)| < l_{\Omega_1,L_1}|g(\omega_1,\Omega_1)| = l_{\Omega_2,L_1}|g(\omega_1,\Omega_2)| \\ |g(\omega_2,\Omega)| > l_{\Omega_1,L_2}|g(\omega_2,\Omega_1)| = l_{\Omega_2,L_2}|g(\omega_2,\Omega_2)| \end{cases}. \tag{35}$$

If the MSR system is stable at a given rotor speed, then the rotor stable region can be solved by (35).

### 6.2. Example 4

As for Example 3 in Section 5, the crossing frequencies, as well as the corresponding gains, are given in Table 6. As shown in the figure, the varying rotor speed does not affect the crossing frequencies, but it changes the gains at these frequencies.

Table 6. Crossing frequencies and the corresponding gains

| Rotor Speed | Crossing Frequencies | Gains |
|---|---|---|
| 3000rpm | $\omega_1 = -22\text{rad/s}$ | $l_{\Omega_1,1} = 1.85$ |
| | $\omega_2 = 8010\text{rad/s}$ | $l_{\Omega_1,2} = 0.504$ |
| 12000rpm | $\omega_1 = -22\text{rad/s}$ | $l_{\Omega_1,1} = 1.67$ |
| | $\omega_2 = 8010\text{rad/s}$ | $l_{\Omega_1,2} = 0.584$ |

Substituting the crossing frequencies and their corresponding gains into (35) yields

$$\begin{cases} |g(-22,\Omega)| < 1.85|g(-22,3000\text{rpm})| \\ |g(8010,\Omega)| > 0.504|g(8010,3000\text{rpm})| \end{cases}. \quad (36)$$

By solving the inequations (36), the positive rotor speed stable region is $[0\text{rpm}, 3.58\times10^4\text{rpm})$. Accordingly, the negative rotor speed stable region is $(-3.58\times10^4\text{rpm}, 0\text{rpm}]$. Thus the rotor speed stable region is $(-3.58\times10^4\text{rpm}, 3.58\times10^4\text{rpm})$. In fact, we can get the equation below from (31)

$$l_{\Omega,L_i} = \frac{|g(\omega_i,\Omega_0)|}{|g(\omega_i,\Omega)|} l_{\Omega_0,L_i}. \quad (37)$$

Thus,

$$\begin{cases} l_{\Omega,L_1} = \dfrac{|g(\omega_1,\Omega_2)|}{|g(\omega_2,\Omega)|} l_{\Omega_2,L_1} \\ l_{\Omega,L_2} = \dfrac{|g(\omega_1,\Omega_2)|}{|g(\omega_2,\Omega)|} l_{\Omega_2,L_2} \end{cases}, \quad (38)$$

where $\Omega_2 = 3000\text{rpm}$, the gains at the crossing frequencies $\omega_1$ and $\omega_2$ under different rotor speeds are shown in Figure 10.

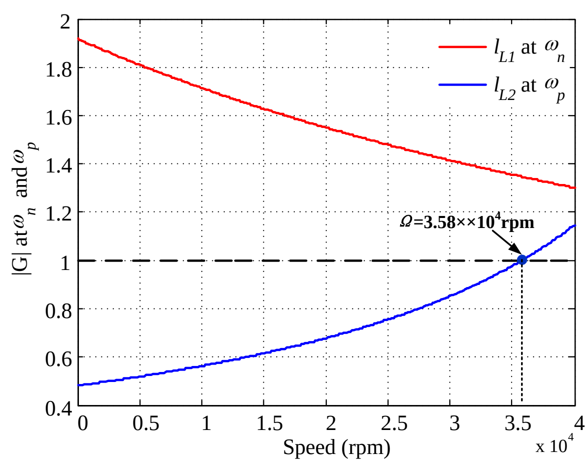


Figure 10. Gains at crossing frequencies under different rotor speeds

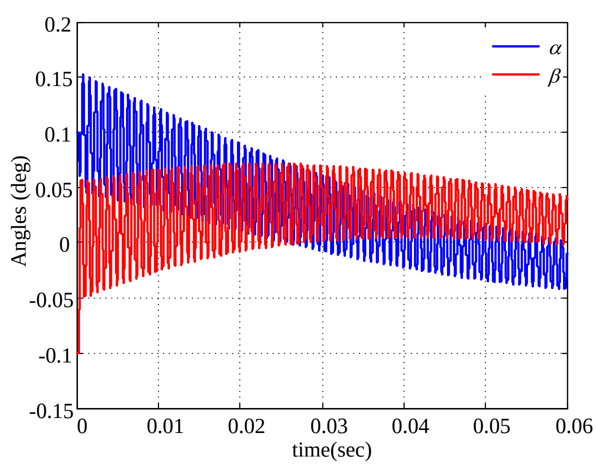


(a) Ω =35000rpm

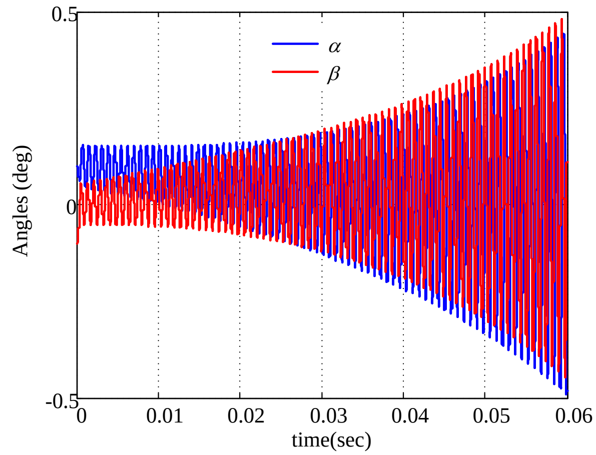


(b) Ω =36000rpm

Figure 11. Simulation results at speeds below and above the critical stable speed respectively

The MSR system will arrive at a critical stable status when the rotor speed is approximately 3.58×10⁴ rpm at 8010 rad/s. And it will lose stability if the speed continues to increase. The simulation results are shown in Figure 11 (a) and (b) at a speed of $3.5\times10^4\text{rpm}$ below the critical stable speed and at a speed of $3.6\times10^4\text{rpm}$ above the critical stable speed, respectively.

## 7. Conclusion

This paper presents a novel approach to study the absolute and relative stabilities for MSRs in the frequency domain. Several important theories and methods are proposed, including the equivalent stability relationship between the single complex variable and the two traditional real deflection angles, the extended Nyquist criterion for complex coefficient transfer functions, the absolute stability theorem for MSRs with centralized PID plus cross-feedback controller and the method to calculate the rotating speed stable region. The methods and theories in this paper make it easier and more systematical to study the stability for MSRs and examples and simulations are employed to demonstrate them. Moreover, the extended Nyquist criterion is also valid to a wider class of systems with a similar dynamic model.

## References


[1]. Schweitzer G, Maslen EH. Magnetic bearings: theory, design, and application to rotating machinery. Springer, Berlin, Germany, 2009.

[2]. Dever T, Brown G, Duffy K, Jansen R. Modeling and Development of Magnetic Bearing Controller for High Speed Flywheel System. The 2nd International Energy Conversion Engineering Conference, Providence, USA, Aug. 2004.

[3]. Polajžer B, Ritonja J, Štumberger G, Dolinar D, Lecointe J-P. Decentralized PI/PD position control for active magnetic bearings. Electrical Engineering. 2006, 89, 53-59.

[4]. Psonis TK, Nikolakopoulos PG, Mitronikas E. Design of a PID Controller for a Linearized Magnetic Bearing. International Journal of Rotating Machinery. 2015. DOI:

10.1155/2015/656749.
[5]. Ahrens M, Kucera L, Larsonneur R. Performance of a magnetically suspended flywheel energy storage device. IEEE Transactions on Control Systems Technology. 1996, 4, 494-502.
[6]. Kai X, Kun L, Xiaoqiang S. Study on Cross Feedback Control of Magnetic Bearing Based on Root Locus. The 2nd Chinese Symposium on Magnetic Bearings, Nanjing City, China, Aug. 2007.
[7]. Ren Y, Fang J. Complex-Coefficient Frequency Domain Stability Analysis Method for a Class of Cross-Coupled Antisymmetrical Systems and Its Extension in MSR Systems. Mathematical Problems in Engineering. 2014. DOI: 10.1155/2014/765858.
[8]. Ren Y, Fang J. Modified Cross Feedback Control for a Magnetically Suspended Flywheel Rotor with Significant Gyroscopic Effects. Mathematical Problems in Engineering. 2014. DOI: 10.1155/2014/325913.
[9]. Brown GV, Kascak AF, Jansen RH, Brown GV, Kascak AF. Stabilizing Gyroscopic Modes in Magnetic Bearing-Supported Flywheels by Using Cross-Axis Proportional Gains. AIAA Journal. 2005.
[10]. Ren Y, Chen X, Cai Y, Wang W. Rotation Modes Stability Analysis and Phase Compensation for Magnetically Suspended Flywheel Systems with Cross Feedback Controller and Time Delay. Mathematical Problems in Engineering. 2016. DOI: 10.1155/2016/3783740.
[11]. Shafai B, Beale S, Larocca P, Cusson E. Magnetic bearing control systems and adaptive forced balancing. IEEE Control Systems. 1994, 14, 4-13.
[12]. Fujita M, Hatake K, Matsumura F. Loop shaping based robust control of a magnetic bearing. IEEE Control Systems. 1993, 13, 57-65.
[13]. Fujita M, Hatake K, Matsumura F, Uchida K. Experiments on the loop shaping based H ∞ , control of a magnetic bearing. American Control Conference, San Francisco, USA, 1993.
[14]. Fang J, Ren Y. High-Precision Control for a Single-Gimbal Magnetically Suspended Control Moment Gyro Based on Inverse System Method. IEEE Transactions on Industrial Electronics. 2011, 58, 4331-4342.
[15]. Fang J, Ren Y. Decoupling Control of Magnetically Suspended Rotor System in Control Moment Gyros Based on an Inverse System Method. IEEE/ASME Transactions on Mechatronics. 2012, 17, 1133-1144.
[16]. Lee CW, Jeong HS. Dynamic modeling and optimal control of cone-shaped active magnetic bearing systems. Control Engineering Practice. 1996, 4, 1393-1403.
[17]. Tombul GS, Banks SP. Nonlinear optimal control of rotating flexible shaft in active magnetic bearings. Science China Technological Sciences. 2011, 54, 1084-1094. 10.1007/s11431-011-4353-9.
[18]. Zhu KY, Xiao Y, Rajendra AU. Optimal control of the magnetic bearings for a flywheel energy storage system. Mechatronics. 2009, 19, 1221-1235.
[19]. Zhang L, Liu K. Riccati difference equation in optimal control for magnetic bearings. Science China Technological Sciences. 2012, 55, 2107-2114.
[20]. Ray K, Kouvaritakis B. An extension of the characteristic sequences method to the case of repeated roots. IEEE Transactions on Automatic Control. 1984, 29, 933-935.
[21]. Fang J, Ren Y, Fan Y. Nutation and Precession Stability Criterion of Magnetically Suspended Rigid Rotors With Gyroscopic Effects Based on Positive and Negative Frequency Characteristics. IEEE Transactions on Industrial Electronics. 2014, 61, 2003-2014.
[22]. Jiang W, Wang H, Wei J. A study of singularities for magnetic bearing systems with time delays. Chaos Solitons & Fractals. 2008, 36, 715-719.
[23]. Zhong P, Townsend MA. Stability of magnetic bearing rotor systems and the effects of gravity and damping. AIAA Journal. 1994, 32, 1492-1499.
[24]. Harnefors L. Modeling of Three-Phase Dynamic Systems Using Complex Transfer Functions and Transfer Matrices. IEEE Transactions on Industrial Electronics. 2007, 54, 2239-2248.
[25]. Zhang K, Zhao L, Zhao H. Research on control of flywheel suspended by active magnetic bearing system with significant gyroscopic effects. Chinese Journal of Mechanical Engineering. 2004, 17, 63-66.
[26]. Fan Y, Fang J. Experimental research on the nutational stability of magnetically suspended momentum wheel in control moment gyroscope (CMG). The 9th International Symposium on Magnetic Bearings, Lexington, USA, Aug., 2004.
[27]. Tong W, Fang JC. Stability Analysis Method of Magnetically Suspended High-Speed Rotor Based on Two-Frequency Bode Diagram. Acta Aeronautica Et Astronautica Sinica. 2007, 28, 641-646.
[28]. Tong W, Fang JC. Proof-phase-margin design of nutation cross-feedback control in magnetically suspended high-speed rotor system with large rotary inertia. Optics & Precision Engineering. 2007, 15, 858-865.
[29]. Ren Y, Su D, Fang J. Whirling Modes Stability Criterion for a Magnetically Suspended Flywheel Rotor With Significant Gyroscopic Effects and Bending Modes. IEEE Transactions on Power Electronics. 2013, 28, 5890-5901.